Article

Biosafety Construction Composite Based on Iron Oxide Nanoparticles and PLGA

Sergey V. Gudkov [1,2,3,], **Dmitriy E. Burmistrov [1]**, **Vasily N. Lednev [1]**, **Aleksander V. Simakin [1]**, **Oleg V. Uvarov [1]**, **Roman N. Kucherov [1]**, **Petr I. Ivashkin [1]**, **Alexey S. Dorokhov [3]** and **Andrey Yu. Izmailov [3]**

[1] Prokhorov General Physics Institute of the Russian Academy of Sciences, 38 Vavilova St., 119991 Moscow, Russia; dmitriiburmistroff@gmail.com (D.E.B.); lednev@kapella.gpi.ru (V.N.L.); avsimakin@gmail.com (A.V.S.); uvarov@kapella.gpi.ru (O.V.U.); rn.kucherov@gmail.com (R.N.K.); ivashkin@kapella.gpi.ru (P.I.I.)

[2] Institute of Biology and Biomedicine, Lobachevsky State University of Nizhni Novgorod, 23 Prospekt Gagarina, 603950 Nizhny Novgorod, Russia

[3] Federal State Budgetary Scientific Institution "Federal Scientific Agroengineering Center VIM" (FSAC VIM), 109428 Moscow, Russia; dorokhov.vim@yandex.ru (A.S.D.); vim@vim.ru (A.Y.I.)

[*] Correspondence: s_makariy@rambler.ru

Abstract: Nanocomposites based on polymers and nanoparticles are used in agriculture for photoconversion of solar radiation, as a basis for covering material, as a packaging material, and as functional films. At the same time, nanocomposites are almost never used in agriculture as biosafe structural materials. In this work, we have developed a technology for obtaining a nanocomposite based on PLGA and iron oxide nanoparticles. The nanocomposite has unique physical and chemical properties and also exhibits pronounced antibacterial properties at a concentration of iron oxide nanoparticles of more than 0.01%. At the same time, the nanocomposite does not affect the growth and development of pepper and is biocompatible with mammalian cells. Nanocomposites based on PLGA and iron oxide nanoparticles can be an attractive candidate for the manufacture of structural and packaging materials in agriculture.

Keywords: iron oxide; poly(lactic-co-glycolic acid); nanoparticles; composite; biocompatibility; antibacterial; cytotoxicity

1. Introduction

The creation of biosafety polymeric materials with antibacterial properties is an important task of modern agricultural science. One of the promising ways to solve this problem is the creation of polymeric materials containing nanoparticles of metals and their oxides, such as Ag_2O [1], ZnO [2], Fe_2O_3, Fe_3O_4 [3], Al_2O_3 [4], TiO_2 [5] and CuO [6]. It is known that nanoparticles of these metals and their oxides have an antibacterial effect against gram-negative and gram-positive bacteria, as well as an antifungal effect [3]. Numerous studies have shown the bacteriostatic and bactericidal effect of Fe_2O_3 and Fe_3O_4 nanoparticles against a wide range of microorganisms [7–9]. It is assumed that the antibacterial action of iron oxide nanoparticles is based on: (1) The ability to generate ROS [10], (2) the ability to inactivate a number of bacterial enzymes [11] and (3) the violation of the integrity of the bacterial cell wall and membrane [12]. At the same time, iron oxide nanoparticles have good biocompatibility in eukaryotes [13] and demonstrate the absence of cytotoxicity or low cytotoxic effect on cell cultures in in vitro experiments [14,15].

For the synthesis of iron oxide nanoparticles, various methods are used, including chemical precipitation [16], the sol-gel method [17], thermal coprecipitation [18], the hydrothermal method [19], laser ablation [20], etc. The laser ablation method allows nanoparticles with desired physicochemical characteristics to be obtained; this method is ideal for primary research [21]. Iron nanoparticles and their oxides are often magnetic; therefore,

colloidal solutions of these nanoparticles tend to agglomerate, which is accompanied by low stability of colloidal solutions and deterioration of biological properties [22]. One of the ways to improve both the physical characteristics of the obtained nanomaterials (colloidal stability, rheological characteristics, photocatalytic properties, etc.) and the biological properties (antibacterial activity, low cytotoxicity, pyrogenicity, etc.) of nanomaterials is the development of polymer-NP composites (borosiloxane [23], gelatin [24], chitosan [25], polyaniline [26], polyurethane [27], poly(lactide-co-glycolide) (PLGA) [28], etc.). Polyaniline, polyurethane and PLGA are fundamentally suitable for structural materials. However, only PLGA is a biocompatible polymer. In the present work, nanocomposites based on PLGA and iron oxide nanoparticles of various concentrations were synthesized. Using the TEM, MIM, DLS, ATM, DSC and spectroscopy methods, the physicochemical properties of the nanocomposite material are characterized. It is shown that the nanocomposite exhibits antibacterial properties. At the same time, the nanocomposite did not have a significant effect on the growth and development of eukaryotes, both of plant and animal origin.

2. Materials and Methods

2.1. Synthesis and Characterization of Nanoparticles

Iron oxide nanoparticles were synthesized using the laser ablation method in deionized water. An iron plate was used as a massive target. A pulsed ytterbium fiber laser was used. The following laser parameters were used: wavelength, 1064 nm; pulse duration, 4–200 ns; pulse repetition rate—20 kHz; average power-up to 20 W; pulse energy—1 mJ. Deionized water was used as the working liquid; the volume was 10 mL. The liquid layer above the target was about 1000–1500 μm. Irradiation time varied in the range from 5 to 20 min. A detailed description of the installation for the generation of nanoparticles by laser ablation can be found in the work of Baimler et al. [29].

The Zetasizer Ultra Red Label (Malvern Panalytical, Malvern, UK) was used to determine the hydrodynamic diameter of the obtained nanoparticles, as well as to obtain the zeta potential distribution. A more detailed description of the features of recording these parameters was described by us earlier [30]. A CPS 24000 disk analytical centrifuge (CPS Instruments, Prairieville, LA, USA) was used to evaluate the diameter of the obtained nanoparticles. The morphological features of nanoparticles (shape, topology), as well as the elemental composition of nanoparticles, were studied using a Libra 200 FE HR transmission electron microscope (Carl Zeiss, Jena, Germany) in combination with a JED-2300 energy-dispersive X-ray spectrometer. To assess the morphological features of the surface of the obtained composite films, a Seiko SII NPX-200 atomic force microscope (Seiko Instruments Inc., Tokyo, Japan) was used. The distribution of nanoparticles in the polymer was assessed using an interference modulation microscope MIM-321 (Amphora Lab, Moscow, Russia). Further, to confirm the composition of the obtained nanoparticles, the spectrum of aqueous colloids of nanoparticles was recorded using a Cintra 4040 differential spectrophotometer (GBC Scientific Equipment, Braeside, Australia).

2.2. Composite Fabrication, Production of Plates from Composite Material, Rheological Properties

The low-temperature technology developed earlier at our research center was used to obtain a composite based on PLGA and iron oxide nanoparticles [31]. The resulting composite material was heated to 40 °C and then rolled through rollers. As a result, a composite film with a thickness of about 1000 μm was obtained. The resulting film was further cut into samples of various sizes. For work with plants, the composite material was heated to 40 °C and then rolled. As a result, composite rods with a diameter of about 0.5 cm were obtained.

2.3. Hydrogen Peroxide Concentration Measurement

The concentration of the formed hydrogen peroxide in aqueous solutions was carried out using a highly sensitive chemiluminescence method [32]. A highly sensitive chemiluminometer was used to register and measure luminescence Biotox-7A-USE (ANO Engineering

Center—Ecology, Moscow, Russia). The calibration and registration procedure is described in detail in a number of our other works. Composite samples were placed in polypropylene vials with the addition of 1 mL prepared before measuring the "counting solution". This solution contained 1 mM Tris-HCl buffer pH 8.5, 50 μM *p*-iodophenol, 50 μM luminol, 10 nM horseradish peroxidase. The sensitivity of this method made it possible to determine H_2O_2 at a concentration of <1 nM [33].

2.4. Hydroxyl Radicals Concentration Measurement

To quantify the content of hydroxyl radicals in aqueous solutions, the reaction with coumarin-3-carboxylic acid (CCA) was used. The hydroxylation reaction produced 7-hydroxycoumarin-3-carboxylic acid (7-OH-CCA), a convenient fluorescent probe for detecting the concentration of OH radicals. To a solution of CCA in water (0.5 mM, pH 3.6) 0.2 M phosphate buffer (pH 7.4) was added. Next, the samples in polypropylene bottles were heated in a thermostat at a temperature of 80.0 ± 0.1 °C for 2 h. A JASCO 8300 spectrofluorimeter (JASCO, Tokyo, Japan) was used to detect fluorescence of 7-OH-CCA at λ_{ex} = 400 nm, λ_{em} = 450 nm. Calibration was carried out using commercial 7-OH-CCA [20].

2.5. Long-Lived Reactive Protein Species Concentration Measurement

Detection of luminescence is an efficient and sensitive method for determining free radical reactions. The interaction of radicals is accompanied by the release of energy in the form of emitted light quanta [34]. In this case, the interaction of radicals releases the energy emitted in the form of light quanta. Chemiluminometer Biotoks-7A (AND "Engineering Center—Ecology", Russia) was used to study long-lived reactive protein species by measuring the chemiluminescence of protein solutions with increasing temperature. The measurements were carried out in the dark at room temperature in 20 mL plastic polypropylene vials. All samples were stored in the dark at room temperature for 30 min after exposure. Protein solutions not subjected to heating were used as controls. A more detailed description of the method was presented in the work of Sharapov et al. [35].

2.6. Enzyme-Linked Immunosorbent Assay (ELISA)

To quantify 8-oxoguanine in DNA, a non-competitive enzyme-linked immunosorbent assay (ELISA) was used using monoclonal antibodies specific for 8-oxoguanine (anti-8-OG antibodies) [36]. DNA samples (350 μg/mL) were denatured by boiling in a water bath for 5 min and cooled on ice for 3–4 min. Aliquots (42 μL) were applied to the bottom of the wells of the ELISA plates. DNA was immobilized using a simple adsorption procedure with incubation for 3 h at 80 °C until the solution was completely dry. Non-specific adsorption sites were blocked with 300 μL of a solution containing 1% skimmed milk powder in 0.15 M Tris-HCl buffer, pH 8.7 and 0.15 M NaCl. Next, the plates were incubated at room temperature overnight (14–18 h). The formation of an antigen-antibody complex with antibodies against ti-8-OG (at a dilution of 1:2000) was carried out in a blocking solution (100 μL/well) by incubation for 3 h at 37 °C. It was washed twice (300 μL/well) with 50 mM Tris-HCl buffer (pH 8.7) and 0.15 M NaCl with 0.1% Triton X-100 after 20 min incubation. Next, the complex with the conjugate (anti-mouse immunoglobulin labeled with horseradish peroxidase (1:1000)) was formed by incubation for 1.5 h at 37 °C in a blocking solution (80 μL/well). The wells were then washed 3 times as described above. Next, a chromogenic substrate containing 18.2 mM ABTS and hydrogen peroxide (2.6 mM) in 75 mM citrate buffer, pH 4.2 (100 μL/well), was added to each well. Reactions were stopped by adding an equal volume of 1.5 mM NaN3 in 0.1 M citrate buffer (pH 4.3) when color was achieved. The optical density of the samples was measured on a plate photometer (Titertek Multiscan, Vantaa, Finland) at λ = 405 nm. The method was described in more detail earlier [37].

2.7. Thermal Analysis

Differential thermal analysis (DTA) and thermogravimetric analysis (TGA) were performed using a SETSYS Evolution TGA-DTA/DSC instrument (SETERAM Instrumentation, France) on the obtained samples of PLGA/iron oxide NP composites. The designated temperature range is from room temperature to 1200 °C. The data were adjusted for baseline by performing a blank test and subtracting it from the original data [38].

2.8. Antibacterial Activity Assay

The antibacterial activity of the obtained PLGA/iron oxide NPs composites was evaluated against gram-negative bacteria *Escherichia coli*. Film samples 10 × 10 mm in size were pre-sterilized by soaking in a 70% ethanol solution for 30 min. Next, the film was put on a sterile hoop, on which a liquid LB nutrient medium with a known number of CFU was placed. The resulting construct was placed in an ES-20 shaker incubator (Biosan, Riga, Latvia) and cultured at 37 °C, at approximately 150 rpm for 24 h. Using microscopy and the previously developed algorithm for detecting optically dense objects in the frame, the concentration of bacterial cells was estimated during the cultivation time. At the end of the experiment, the structure was dismantled, and the concentration of bacteria was assessed using a drop spectrometer [39].

2.9. Determination of Leaf Area

The experiments were carried out in a climate chamber. Plants were grown in soil under standard conditions (illumination 16 h a day, temperature 22 °C). The leaf area of *Capsicum annuum* was changed using the GreenImage software developed by us [40]. The original RGB images of plant leaves were obtained in a vertical position with the same distance from the camera lens to the leaf. To select the pixels corresponding to the image of the leaves, the following green selection procedure was used: $I_G = I_g - aI_r - bI_b$, where I_g, I_r and I_b are the intensities of the RGB color components of the pixel, I_G is the resulting intensity of the selected green and a and b are weight coefficients. Then, a threshold procedure was applied. To estimate the sheet area, the total number of pixels was normalized to the specific area of one pixel [41].

2.10. Cytotoxicity Study

The obtained samples of the PLGA/iron oxide NPs composite films were evaluated for their in vitro cytotoxicity against permanent human neuroblastoma cell lineage SH-SY5Y. These cells are a good model for studying the development and differentiation of nerve cells in vitro. A feature of this cell line is the possibility of their growth both in the monolayer and as aggregates in the volume of the medium [42]. DMEM (Biolot, Moscow, Russia) containing 10% fetal calf serum (Gibco, USA) and 30 µg/mL gentamicin (PanEco, Moscow, Russia) was used as a culture medium. Cultivation was carried out in a CO_2 incubator S-Bt Smart Biotherm (Biosan, Riga, Latvia) at 37 °C and 5% CO_2.

Sterile samples of the PLGA/iron oxide NPs composite 20 × 20 mm in size were placed in Petri dishes Ø 35 mm for each of the samples. A suspension of SH-SY5Y cells (10^4 cells/cm^2, V = 3 mL) was placed on the surface of the samples. The in vitro cultivation time on the surface of the studied films was 72 h. Next, the viability of cell cultures was assessed by staining the cultures with fluorescent dyes Hoechst 33342 (Sigma, St. Louis, MO, USA) and propidium iodide (Sigma, St. Louis, MO, USA) at concentrations of 2 µg/mL each. Hoechst 33342 stains both living and non-viable cells. Propidium iodide stains non-viable cells with a damaged cytoplasmic membrane. This dye penetrates into living cells extremely slowly.

An imaging system based on Leica DMI6000 (Leica, Wetzlar, Germany) was used for microscopic analysis of cells on the surface of PLGA/iron oxide NPs composite samples. At least 500 cells were counted on the film surfaces during the analysis [43]. A number of photographs were taken on a randomly selected field of the culture in question in transmitted light, with filters for Hoechst and propidium iodide. The number of non-viable

cells, the cell culture density, the percentage of cell-free surface area and even the mitotic index was evaluated as the main parameters that determine the growth and development of cells using the ImageJ software. Cell mitotic index scores were used to analyze cell proliferation. Cells in the state of mitosis were identified by the distribution of chromatin stained with Hoechst 33342 (Sigma, St. Louis, MO, USA) characteristic of prophase (P), metaphase (M), anaphase (A) and telophase (T). The mitotic index (MI) was calculated using the formula MI = (P + M + A + T)/N × 100%, where (P + M + A + T) is the number of cells at the prophase, metaphase, anaphase and telophase stages, respectively, and N is the total number of analyzed cells. This method was described in more detail by us earlier [44].

2.11. Statistic

The data were analyzed using GraphPad Prism eight and Origin software and were presented as means ± SEM. Data from at least three independent experiments were used for averaging.

3. Results

Iron oxide nanoparticles were synthesized by laser ablation in water. The concentration and hydrodynamic diameter of the resulting nanoparticles were determined using a Malvern Ultra Red Label instrument. The resulting colloidal solution contained ~4.2×10^9 nanoparticles per ml, the average hydrodynamic diameter of nanoparticles was about 50 nm (Figure 1a). The size distribution of nanoparticles was monomodal with a distribution half-width of about 30 nm. Moreover, the zeta potential of the nanoparticles was determined, which was in the order of +20 mV (Figure 1b). Optical absorption spectra were obtained using a differential spectrophotometer (Figure 1c). The absorption spectra suggest that the nanoparticles probably consist mainly of Fe_2O_3. Morphology analysis was performed using TEM. It was found that all nanoparticles in the colloidal solution had a spherical shape, with an average diameter of about 50 nm (Figure 1d).

Using energy-dispersive X-ray spectroscopy (EDX), the chemical composition of the resulting nanoparticles was determined. The content of two elements in the composition of nanoparticles was revealed: iron and oxygen. It was found that the colloidal solution contained chemically pure nanoparticles without impurities, consisting of iron oxide (Figure 2a–c).

The fabrication of a nanocomposite based on PLGA and nanoparticles from iron oxide was carried out by a low-temperature method developed by us earlier [31]. The resulting composite material visually had a uniform and smooth surface. Using atomic force microscopy, it was found that the surface of the resulting composite is homogeneous and has no cracks, breaks or other artifacts (Figure 3).

To study the location of nanoparticles in the polymer, we used the method of modulation-interference microscopy (MIM), which makes it possible to reveal patterns in materials that differ in refractive index and other optical properties. The refractive index was determined at the wavelength of the laser microscope. The refractive index of the unmodified PLGA is 1.47 at 405 nm, and the refractive index of the Fe_2O_3 is 2.5 at 405 nm. The refractive index of PLGA and iron oxide nanoparticles differ by 60%. It was shown that PLGA, in the absence of nanoparticles, is an optically homogeneous material (Figure 4a). The introduction of iron oxide nanoparticles into the PLGA matrix, even at the lowest concentration (0.001%), led to the formation of domains distinguished by a change in the phase of laser radiation (Figure 4b). Merging of the domains of nanoparticles with the formation of clusters several micrometers in size was noted with an increase in the concentration of iron oxide nanoparticles up to 0.1% (Figure 4c,d). Therefore, it has been shown that the distribution of iron oxide nanoparticles in the PLGA-based composite was uneven, with a pronounced domain structure.
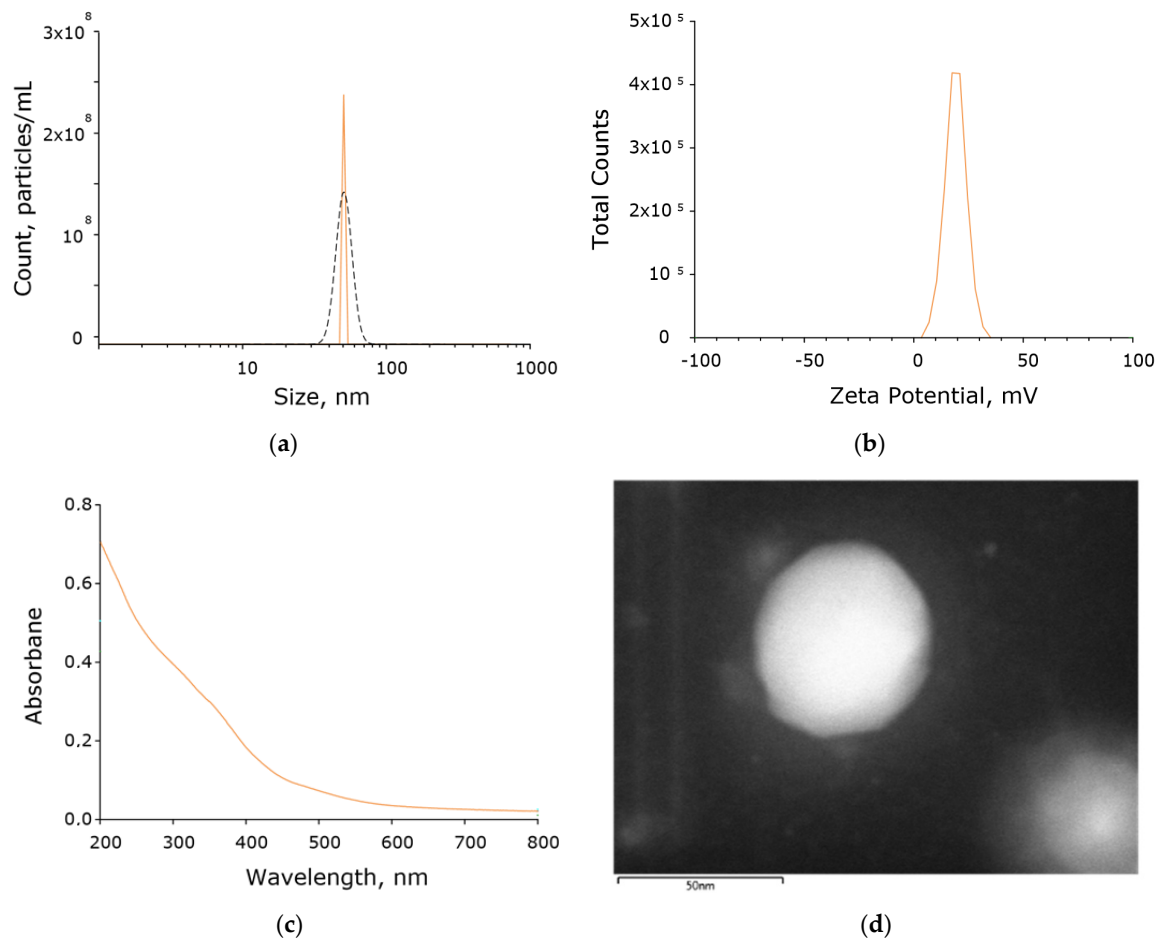
Figure 1. Physicochemical characteristics of a colloidal solution of iron oxide nanoparticles. Concentration (DLS, solid crimson line) and size distribution (CPS, black dashed line) of iron oxide NPs (**a**); zeta potential of iron oxide NPs (**b**); optical absorption spectrum of the obtained colloidal solution of iron oxide nanoparticles (**c**); TEM image of a single iron oxide nanoparticle (**d**).

The thermal analysis of the obtained nanocomposites was carried out. Figure 5 shows the thermograms of the samples obtained in the heating and cooling mode. The numerals indicate different concentrations of iron oxide in the composition of the composite. The addition of iron oxide NPs to PLGA led to a decrease in the glass transition temperature. In the temperature range of 317–320 K, the glass transition process of the composites was observed, which is common for all considered composite samples. Using differential scanning calorimetry, the glass transition temperatures Tg and the change in heat capacity ΔCp of the samples under study were determined (Figure 5b,c). The glass transition temperature is in the range of 317–319 K, which corresponds to the literature data for pure PLGA. The ΔCp values did not change statistically when nanoparticles were added to the PLGA composition. There was a trend towards an increase in the heat capacity of materials.

It is known that iron oxide nanoparticles are capable of generating ROS, mainly in the course of the Fenton and Haber–Weiss reactions [45]. The ability of the synthesized nanocomposite based on PLGA with iron oxide nanoparticles to generate such ROS as hydrogen peroxide and hydroxyl radicals was studied. It was shown that pure PLGA had no effect on the generation of ROS in aqueous solutions. When iron oxide nanoparticles appear in PLGA, an increase in the rate of formation of both hydrogen peroxide (Figure 6a) and hydroxyl radicals (Figure 6b) is observed. An increase in the concentration of iron oxide nanoparticles in the composition of the composite contributed to an increase in the rate of ROS generation. In particular, composites with the highest concentration of iron

oxide nanoparticles of 0.1% contributed to an increase in the formation of H_2O_2 by ~6 times and OH radicals by ~7 times compared with the control values.

(a)

(b)

(c)
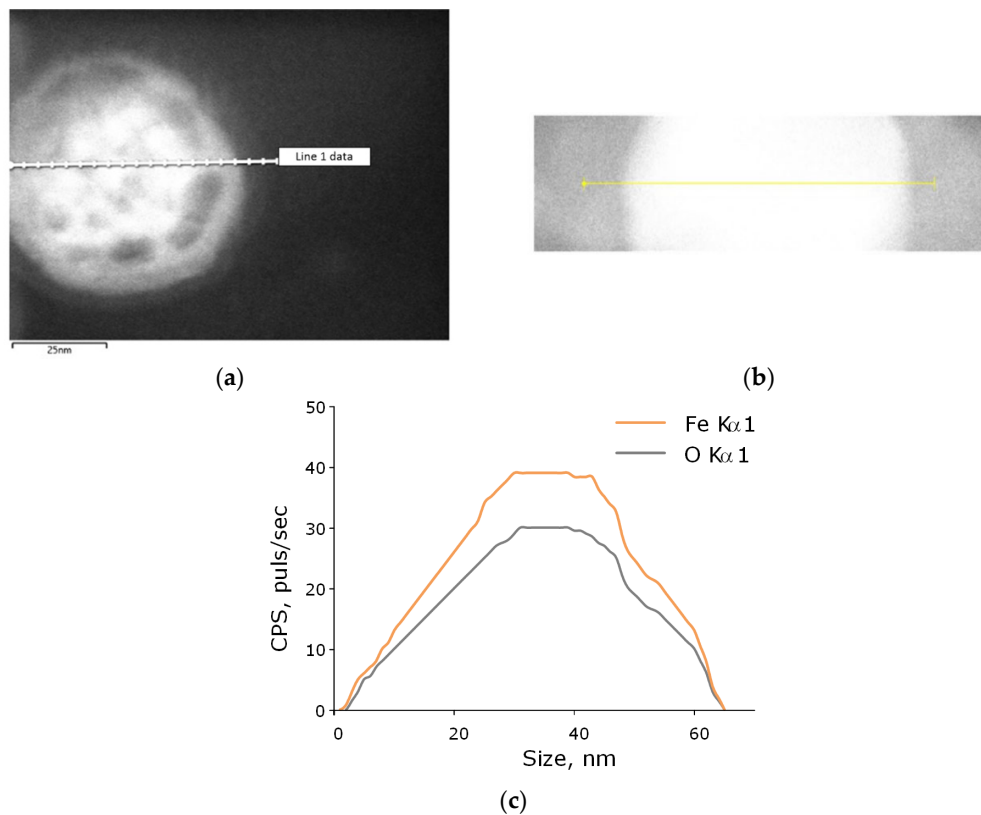
Figure 2. Elemental analysis of iron oxide NPs. (**a**) TEM image of a single iron oxide NP, analysis section is indicated by line 1. (**b**) Enlarged measurement site. (**c**) Nanoparticle profile by Fe Kα1 and O Kα1.


(a)

(b)
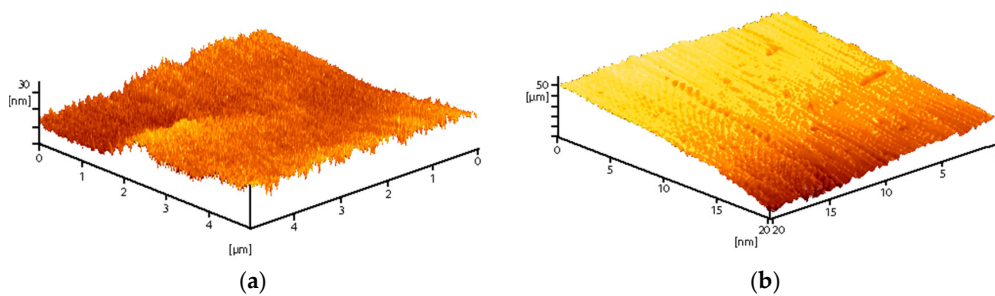
Figure 3. Images of the surface of a composite material obtained using atomic force microscopy with different resolutions (**a**) high, (**b**) low.
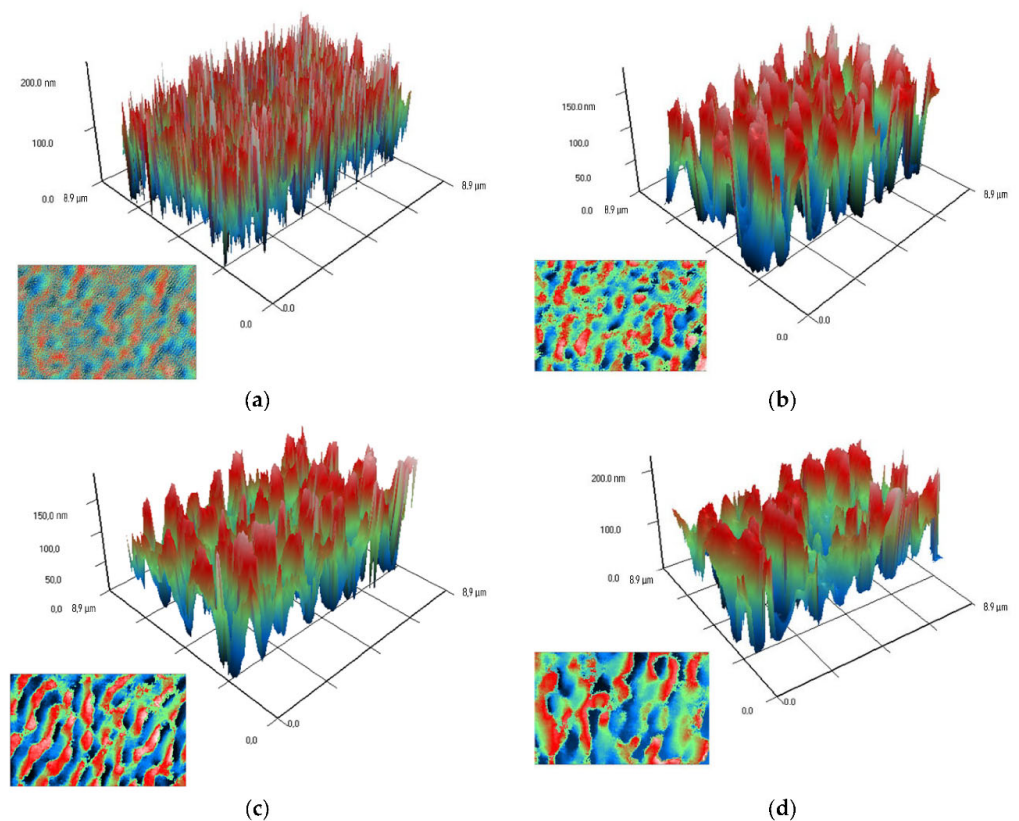
Figure 4. Modulation-interference images of nanocomposites with different dopant content in the composition (pure PLGA (**a**), nanoparticles 0.001% (**b**), 0.01% (**c**) and 0.1% (**d**)). X and Y-axis frame size (μm); Z-axis phase incursion (nm). The image in the lower left corner for each figure is a plan view projection showing the dopant distribution in the matrix.

It is known that high concentrations of ROS lead to damage to biopolymers, in particular DNA. We have studied the effect of a material based on PLGA with iron oxide nanoparticles on the formation of 8-oxoguanine in DNA in vitro. It was found that under PLGA conditions without nanoparticles, it did not affect the rate of 8-oxoguanine formation in DNA. With the appearance of iron oxide nanoparticles in PLGA, an increase in the rate of formation of 8-oxoguanine in DNA was observed in proportion to the increase in the concentration of nanoparticles. At a concentration of nanoparticles of 0.001%, an increase in the rate of formation of 8-oxoguanine in DNA by 1.5 times was observed; at a concentration of nanoparticles of 0.01%, 6 times; at a concentration of 0.1%, ~12 times (Figure 7a).

(a)

(b)

(c)
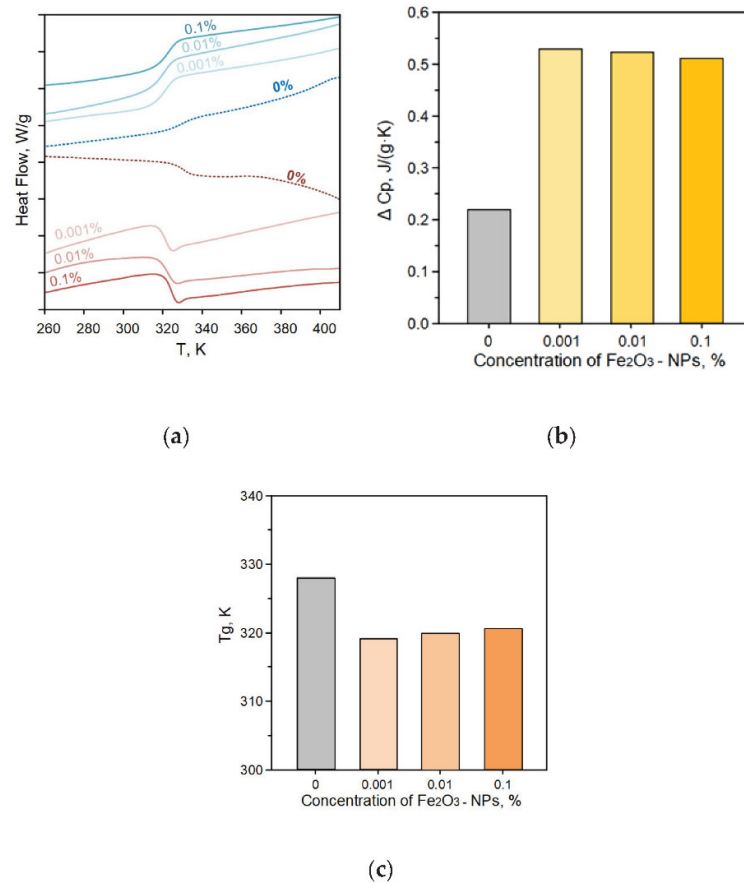
Figure 5. Results of thermal analysis of synthesized composite materials; (**a**) thermograms obtained in the mode of heating and cooling of the material based on PLGA and iron oxide nanoparticles with different concentrations; (**b**) and (**c**) dependences of the heat capacity and glass transition temperature on the concentration of nanoparticles in the samples.


(a)

(b)
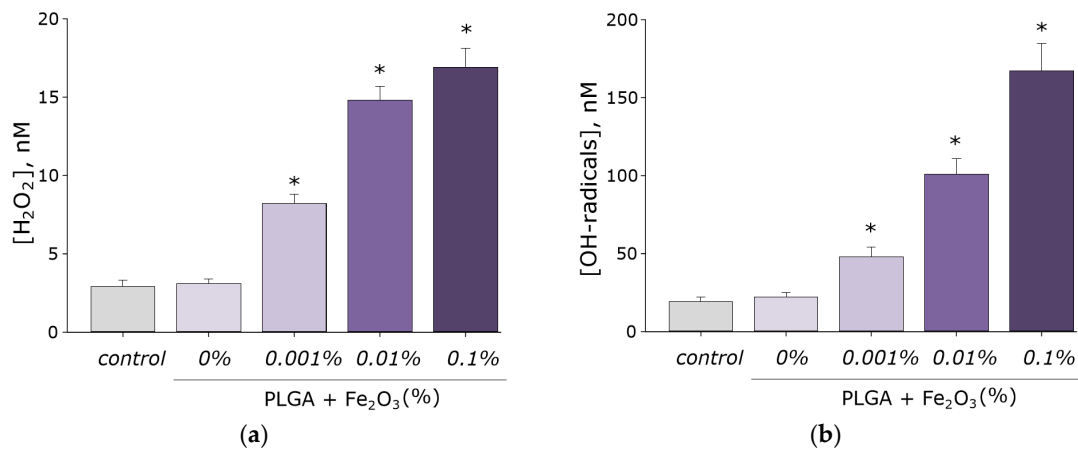
Figure 6. Effect of a PGLA-based material with iron oxide nanoparticles on the generation of ROS in aqueous solutions: hydrogen peroxide (**a**), hydroxyl radicals (**b**). *—statistically significant differences compared with the control group ($p < 0.05$). Data are presented as mean ± standard error of the mean.

(a)

(b)
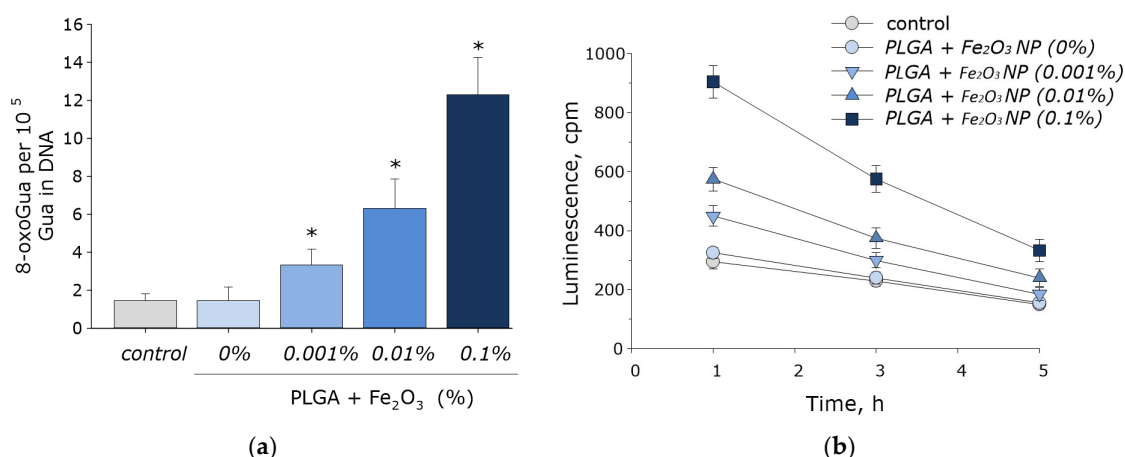
Figure 7. Effect of PGLA-based material with iron oxide nanoparticles on the formation of 8-oxoguanine in DNA (**a**) and the dynamics of the formation of active long-lived forms of proteins (**b**). *—statistically significant differences compared with the control group ($p < 0.05$). Data are presented as mean ± standard error of the mean.

The effect of a material based on PLGA with iron oxide nanoparticles on the formation of long-lived reactive protein species has been studied. PLGA, which does not contain nanoparticles in its composition, did not affect either the rate of generation of long-lived reactive protein species or their half-life. Doping of the polymer with iron oxide nanoparticles resulted in a statistically significant increase in the rate of formation of long-lived reactive protein species (Figure 7b). At the same time, the addition of nanoparticles did not significantly affect the half-life of proteins, which was about 4–5 h.

The obtained nanocomposites were studied for the growth and development of *E. coli* bacterial cultures. PLGA without the addition of iron oxide nanoparticles had no effect on the growth and development of bacterial cells. The addition of iron oxide nanoparticles to PLGA led to a sharp decrease in the number of bacterial cells. An increase in the concentration of nanoparticles led to an increase in the antibacterial effect. The number of cells in contact with composites containing 0.001% nanoparticles was reduced by approximately 35%; with 0.01%, approximately 5.2 times. The PLGA composite containing 0.1% iron oxide nanoparticles had the most pronounced bacteriostatic properties (Figure 8).
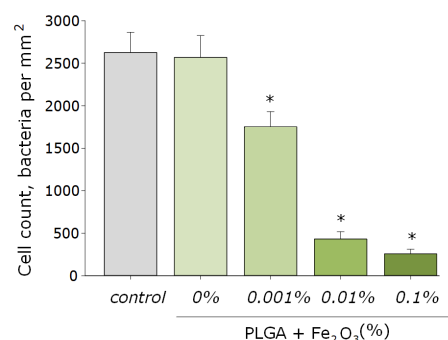
Figure 8. Influence of composite material based on PLGA and iron oxide nanoparticles on the growth and development of *E. coli*. *—indicates a significant difference at 5% level in comparison with the control ($p < 0.05$). Data are presented as mean values and standard errors of the mean.
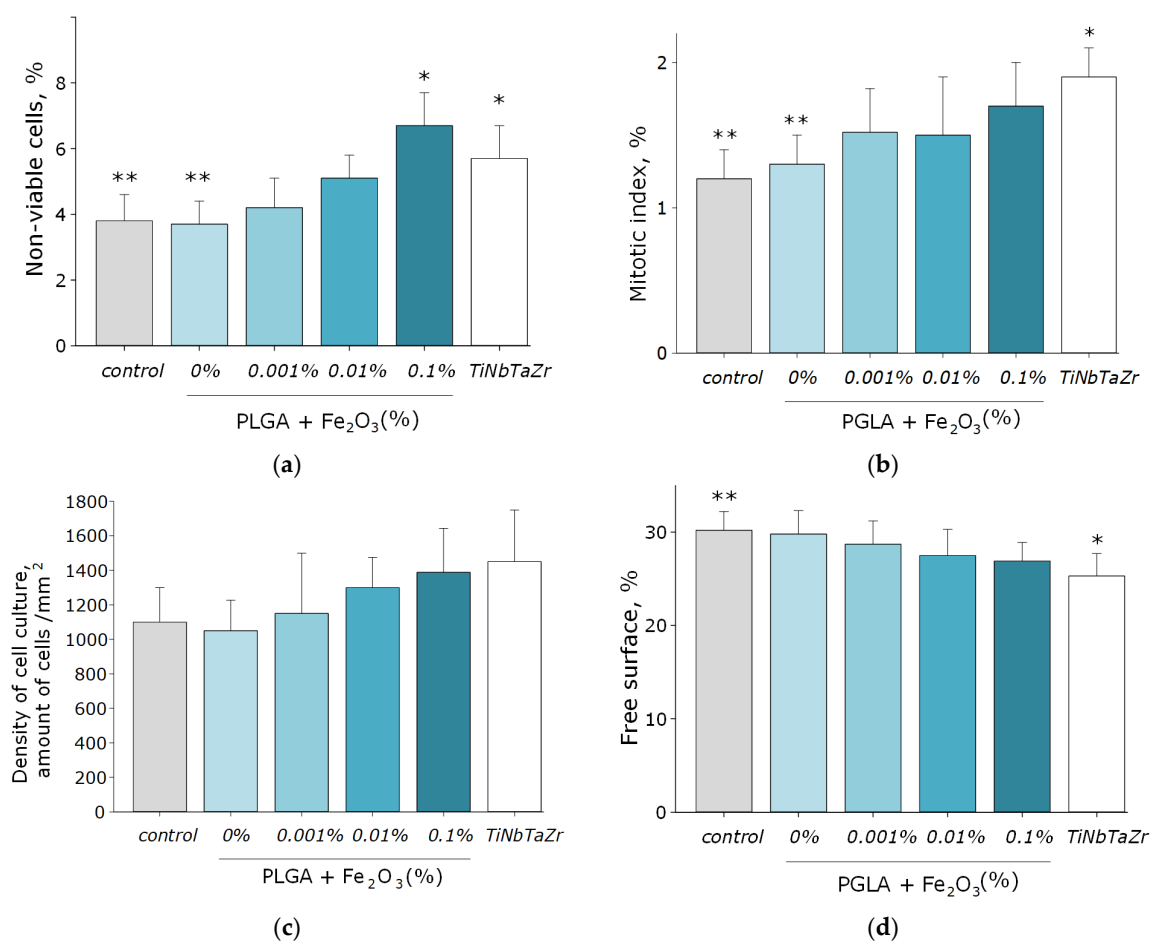
The effect of a nanocomposite based on PLGA and iron oxide nanoparticles on the growth rate of peppers (*Capsicum annuum*) has been studied. The growth rate was determined by the leaf area. A nanocomposite rod with a diameter of 0.5 cm was stuck into the soil to the entire depth of the vessel with soil at the rate of one rod per 10 cm^2 of soil

area. It was shown that neither PLGA without nanoparticles nor PLGA with iron oxide nanoparticles affected the growth rate of Capsicum annuum (Figure 9).

(**a**)   (**b**)
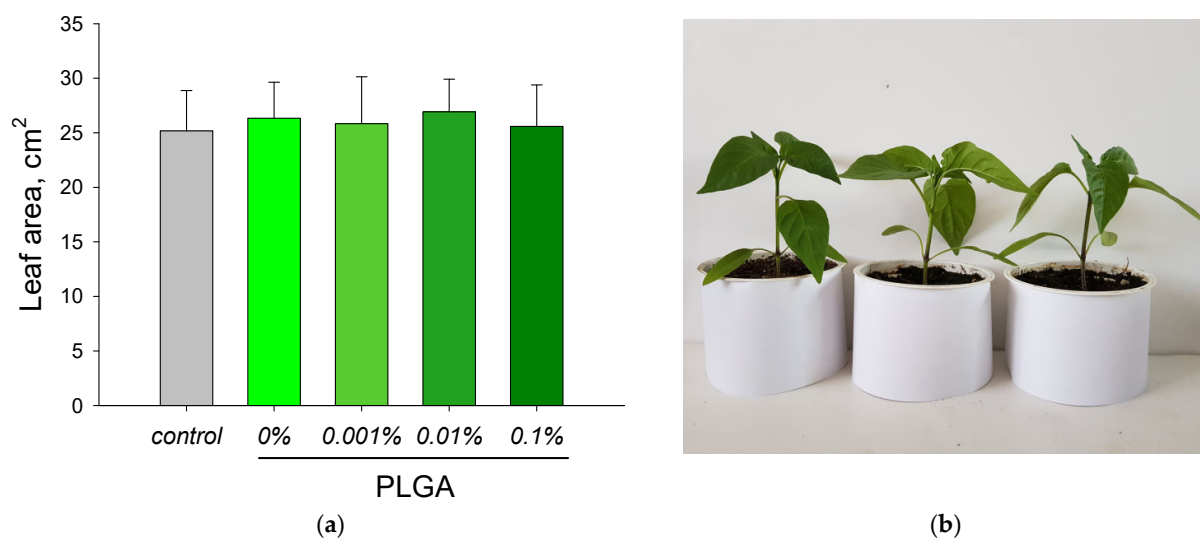
Figure 9. Influence of a nanocomposite based on PLGA and iron oxide nanoparticles on the leaf size of *Capsicum annuum* pepper plants (**a**). Data are presented as mean values and standard errors of the mean. On the right is a comparative photograph of random plants from groups (1) Control, (2) PLGA without nanoparticles and (3) PLGA with 0.1% iron oxide nanoparticles (**b**).

The cytotoxic effect of the material based on PLGA with iron oxide nanoparticles was studied in vitro against the SH-SY5Y cell line (Figure 10a–d). It was shown that the growth rate of cell cultures on the surface of the culture plastic (control group) was worse than on the surface of the medical alloy (TiNbTaZr group). This was manifested in a statistically significant decrease in the % of mitosis events and a lower surface area occupied by cells in the control group. When using PLGA without iron oxide nanoparticles (group 0%) as a surface for cell growth, all parameters under consideration did not change and were at the level of the "control" group. About 4% of non-viable cells were present in cultures; ~1.3% of cells showed mitotic activity; the culture density was ~1000 cells/mm^2, ~30% of the area of the composite sample was occupied by cells. The formation of a single monolayer was not observed. Doping of PLGA with iron oxide nanoparticles led to an increase in the percentage of non-viable cells. When using the nanocomposite with the highest concentration of iron oxide nanoparticles (group 0.1%), a statistically significant increase in the proportion of non-viable cells in cultures (~7%) was revealed. Other indicators did not change; there was a tendency to increase the density of cell cultures, as well as the proportion of cells showing mitotic activity. Thus, it was found that the surface of nanocomposites is suitable for the adhesion, growth and development of eukaryotic cells of the SH-SY5Y line.

Figure 10. Results of evaluation of the cytotoxic effect of the nanocomposite based on PLGA with iron oxide nanoparticles on cultures of eukaryotic cells of the SH-SY5Y line. Proportion of non-viable cells in culture (**a**); mitotic index (**b**); cell culture density (**c**); surface of the composite free of cells (**d**). *—statistically significant differences compared with the control group ($p < 0.05$). **—statistically significant differences compared with the "TiNbTaZr" group ($p < 0.05$). Data are presented as mean $\pm$ standard error of the mean.

4. Discussion

We have obtained nanoparticles of iron oxide (III) by laser ablation in water. A competitive method for obtaining iron oxide nanoparticles is the thermal decomposition of iron salts or their complexes (oleate, acetylacetonate, N-nitrosophenylhydroxylamine or iron carbonyl) in the presence of reducing agents and stabilizing agents [46–48]. If the metal in the compound is in oxidation state 0, then decomposition will result in a simple substance, which is then oxidized to the mixed-valence state Fe^{2+}/Fe^{3+}. As a result, homogeneous nanoparticles with a narrow size distribution are obtained. The advantage of the thermal decomposition method is the possibility of mass production of nanoparticles. The disadvantage of this method is the synthesis in an organic solvent and as a result, the need for an additional stage—the transfer of nanoparticles from the organic to the aqueous phase, since aqueous solutions of nanoparticles are used for biomedical and agricultural applications.

The TEM method showed that these nanoparticles had a spherical morphology (Figure 1d). DLS analysis showed that the colloidal solutions of the synthesized nanoparticles are monodisperse and stable (Figure 1a,b). X-ray spectroscopy confirmed that the obtained nanomaterials have a high chemical purity (Figure 2). These nanoparticles were successfully loaded into a PLGA polymer matrix using an efficient low-temperature method previously developed by our team. The surface of the obtained films was visually homogeneous, without significant defects (Figure 3). Using modulation-interference microscopy, it

was found that the iron oxide nanoparticles are distributed unevenly in the PLGA matrix, forming domain structures (Figure 4). The size of the domain increased with an increase in the concentration of nanoparticles in the polymer. Thermal analysis of the obtained PLGA/iron oxide NP's composites showed that the addition of iron oxide nanoparticles to PLGA leads to a decrease in the glass transition temperature of the composite (Figure 5c). The increase in the concentration of nanoparticles in the composition of the material does not affect the change in the glass transition temperature. The heat capacity did not change when iron oxide nanoparticles were added to the polymer matrix and was within the error (Figure 5b).

The formation of reactive oxygen species is one of the main mechanisms of the antibacterial action of iron oxide nanoparticles [49,50]. Fe^{2+} ions released by nanoparticles react with ROS in accordance with the Fenton equations with the formation of free hydroxyl radicals [10]. High concentrations of ROS damage cell biopolymers in a process called oxidative stress, which leads to its further death [51]. One of the results of such damage is the formation of 8-oxoguanine in DNA, which promotes the formation of mismatched nucleotides with adenine [52]. It was found that the resulting PLGA/iron oxide NPs composite increases the rate of formation of hydrogen peroxide and hydroxyl radicals by several times (Figure 6a,b). The concentration of ROS formed increased as the concentration of nanoparticles in the composite composition increased. Moreover, it was found that this composite material promotes the formation of 8-oxoguanine in DNA in vitro (Figure 7a) and long-lived forms of proteins (Figure 7b). Pure PLGA was found to have no effect on bacterial cell growth. The use of a composite material containing even the lowest concentration of iron oxide nanoparticles had a bacteriostatic effect (Figure 8). At present, a significant number of studies devoted to the successful creation of composite materials based on polymers and iron oxide nanoparticles have been accumulated [3]. Some of these studies are presented in Table 1. In several works, the authors noted a higher antibacterial potential of iron oxide nanoparticles in combination with a polymer component compared to pure nanoparticles. It is also important to note that the composite material we developed did not have a significant effect on the growth and development of plants (Figure 9) and cell cultures (Figure 10a–d). All considered parameters were kept at the proper level.

Table 1. Bacteriostatic properties of composites based on polymers and iron oxide NPs reported in other studies. BS—bacteriostatic effect, BC—bactericidal effect, FS—fungistatic.

Composition	Size of NPs, nm	Bacterial Strains	Effect	MIC/MBC	Results	References
polyaniline (PANI)/iron oxide Fe_3O_4-NPs	~20	*E. coli*, *S. aureus*	BS	-	inhibition of bacterial growth was enhanced by the combined use of PANI Fe_3O_4 compared to pure PANI	[26]
chitosan coated Fe_3O_4-NPs	1.4 ± 5.2	Bacteria: *E. coli*, *B. subtilis*; Fungi: *F. solani*, *A. niger*, *C. albicans*	BS, FS	-	the effect of chitosan-coated Iron oxide nanoparticles was *F. solani*/*A. niger* < *C. albicans* < *E. coli*/*B. subtilis*	[53]
Fe_3O_4-NPs /polyguanidine nanocomposite	~30	*E. coli*	BS	-	nanocomposite exhibited strong antibacterial activity against *E. coli*	[54]
Fe_2O_3-NPs /chitosan (CH) nanocomposite	~30	*E. coli*, *S. aureus*	BS	-	more active growth inhibition of *E. coli* compared to *S. aureus*	[55]
FeO -NPs /chitosan nanocomposite	50–120	*E. coli*, *B. subtilis*, *S. aureus*	BS	-	higher antibacterial effect of the CH/FeO composite as compared to pure FeO NPs	[25]

Table 1. *Cont.*

Composition	Size of NPs, nm	Bacterial Strains	Effect	MIC/MBC	Results	References
FeO -NPs /chitosan nanocomposite	20–22	*Escherichia coli KL226*	BS	MIC: 8 mg/mL	CH/Fe_3O_4 showed more resistive bactericidal effect against *E. coli* species up to 8 mg/mL	[56]
Hyperbranched polyurethane (HBPU)/Fe_3O_4 -NPs	-	*S. aureus, K. pneumonia*	BS	-	activity increases with increasing concentration of nanoparticles	[57]
Hyperbranched polyurethane (HBPU)/Fe_3O_4-NPs nanocomposites decorated multiwall carbon nanotubes (MWCNTs) nanohybrid	~11	*K. pneumonia, S. aureus MTCC96*	BS	-	this nanocomposite accelerated the wound healing process with enhanced wound closure rate, good antibacterial activity	[27]
Fe_3O_4 -NPs coated with catechol-conjugated poly(vinylpyrrolidone) sulfobetaines (C-PVPS)	20–25	*S. aureus ATCC 25424, E. coli ATCC 25922*	BC	-	developed NIR-irradiated photothermal antibacterial nanoparticles	[58]
Fe_2O_3/Fe_3O_4 -NPs modified with quaternarized N-halamine based cationic polymer (CPQN)	2.08 ± 1.7	*E. coli, S. aureus*	BC	-	rapid bactericidal performance for both *E. coli* and *S. aureus*	[59]

5. Conclusions

A new nanocomposite material based on PLGA and iron oxide nanoparticles has been synthesized. For this, iron oxide nanoparticles were obtained by laser ablation in water. The resulting nanoparticles had unimodal distributions. It is shown that the temperature properties (glass transition temperature and thermal conductivity) of the synthesized materials depend on the concentration of introduced nanoparticles. The resulting nanocomposite significantly inhibited the growth and development of bacterial cells, while the nanocomposite did not affect the growth and development of plant and animal cells. The resulting nanocomposite can be a promising candidate for the manufacture of structural materials and packaging in agriculture.

Author Contributions: Conceptualization, D.E.B., A.S.D. and S.V.G.; investigation, D.E.B., V.N.L., A.V.S., O.V.U., R.N.K. and P.I.I.; writing—original draft preparation, D.E.B. and S.V.G.; supervision—A.Y.I. All authors have read and agreed to the published version of the manuscript.

Institutional Review Board Statement: Not applicable.

Informed Consent Statement: Not applicable.

Data Availability Statement: The raw data supporting the conclusions of this article will be made available by the authors, without undue reservation.

Conflicts of Interest: The authors declare no conflict of interest.

References

1. Sotiriou, G.A.; Pratsinis, S.E. Antibacterial activity of nanosilver ions and particles. *Environ. Sci. Technol.* **2010**, *44*, 5649–5654. [CrossRef] [PubMed]
2. Gudkov, S.V.; Burmistrov, D.E.; Serov, D.A.; Rebezov, M.B.; Semenova, A.A.; Lisitsyn, A.B. A Mini Review of Antibacterial properties of ZnO nanoparticles. *Front. Phys.* **2021**, *9*, 641481. [CrossRef]
3. Gudkov, S.V.; Burmistrov, D.E.; Serov, D.A.; Rebezov, M.B.; Semenova, A.A.; Lisitsyn, A.B. Do Iron Oxide Nanoparticles Have Significant Antibacterial Properties? *Antibiotics* **2021**, *10*, 884. [CrossRef] [PubMed]
4. Manogar, P.; Morvinyabesh, J.E.; Ramesh, P.; Jeyaleela, G.D.; Amalan, V.; Ajarem, J.S.; Allam, A.A.; Khim, J.S.; Vijayakumar, N. Biosynthesis and antimicrobial activity of aluminium oxide nanoparticles using Lyngbya majuscula extract. *Mater. Lett.* **2021**, *311*, 131569. [CrossRef]
5. Mahboob, S.; Nivetha, R.; Gopinath, K.; Balalakshmi, C.; Al-Ghanim, K.A.; Al-Misned, F.; Ahmed, Z.; Govindarajan, M. Facile synthesis of gold and platinum doped titanium oxide nanoparticles for antibacterial and photocatalytic activity: A photodynamic approach. *Photodiagn. Photodyn. Ther.* **2021**, *33*, 102148. [CrossRef]
6. Ramzan, M.; Obodo, R.M.; Mukhtar, S.; Ilyas, S.; Aziz, F.; Thovhogi, N. Green synthesis of copper oxide nanoparticles using Cedrus deodara aqueous extract for antibacterial activity. *Mater. Today Proc.* **2021**, *36*, 576–581. [CrossRef]
7. Tran, N.; Mir, A.; Mallik, D.; Sinha, A.; Nayar, S.; Webster, T.J. Bactericidal effect of iron oxide nanoparticles on Staphylococcus aureus. *Int. J. Nanomed.* **2010**, *5*, 277.
8. Behera, S.S.; Patra, J.K.; Pramanik, K.; Panda, N.; Thatoi, H. *Characterization and Evaluation of Antibacterial Activities of Chemically Synthesized Iron Oxide Nanoparticles*; University of Embu: Embu, Kenya, 2012.
9. Ismail, R.A.; Sulaiman, G.M.; Abdulrahman, S.A.; Marzoog, T.R. Antibacterial activity of magnetic iron oxide nanoparticles synthesized by laser ablation in liquid. *Mater. Sci. Eng. C* **2015**, *53*, 286–297. [CrossRef]
10. Fenton, H.J.H. LXXIII.—Oxidation of tartaric acid in presence of iron. *J. Chem. Soc. Trans.* **1894**, *65*, 899–910. [CrossRef]
11. Lee, C.; Kim, J.Y.; Lee, W.I.; Nelson, K.L.; Yoon, J.; Sedlak, D.L. Bactericidal effect of zero-valent iron nanoparticles on Escherichia coli. *Environ. Sci. Technol.* **2008**, *42*, 4927–4933. [CrossRef]
12. Li, Y.; Yang, D.; Wang, S.; Li, C.; Xue, B.; Yang, L.; Shen, Z.; Jin, M.; Wang, J.; Qiu, Z. The Detailed Bactericidal Process of Ferric Oxide Nanoparticles on *E. coli. Molecules* **2018**, *23*, 606. [CrossRef]
13. Hanini, A.; Schmitt, A.; Kacem, K.; Chau, F.; Ammar, S.; Gavard, J. Evaluation of iron oxide nanoparticle biocompatibility. *Int. J. Nanomed.* **2011**, *6*, 787–794. [CrossRef]
14. Feng, Q.; Liu, Y.; Huang, J.; Chen, K.; Huang, J.; Xiao, K. Uptake, distribution, clearance, and toxicity of iron oxide nanoparticles with different sizes and coatings. *Sci. Rep.* **2018**, *8*, 2082. [CrossRef]
15. Calero, M.; Gutiérrez, L.; Salas, G.; Luengo, Y.; Lázaro, A.; Acedo, P.; Morales, M.P.; Miranda, R.; Villanueva, A. Efficient and safe internalization of magnetic iron oxide nanoparticles: Two fundamental requirements for biomedical applications. *Nanomed. Nanotechnol. Biol. Med.* **2014**, *10*, 733–743. [CrossRef]
16. Lassoued, A.; Dkhil, B.; Gadri, A.; Ammar, S. Control of the shape and size of iron oxide (α-Fe$_2$O$_3$) nanoparticles synthesized through the chemical precipitation method. *Results Phys.* **2017**, *7*, 3007–3015. [CrossRef]
17. Akbar, S.; Hasanain, S.; Azmat, N.; Nadeem, M. Synthesis of Fe$_2$O$_3$ nanoparticles by new Sol-Gel method and their structural and magnetic characterizations. *arXiv* **2004**, arXiv:Preprint cond-mat/0408480.
18. Hui, B.H.; Salimi, M.N. Production of iron oxide nanoparticles by co-precipitation method with optimization studies of processing temperature, pH and stirring rate. In Proceedings of the IOP Conference Series: Materials Science and Engineering, Chennai, India, 16–17 September 2020; p. 012036.
19. Ge, S.; Shi, X.; Sun, K.; Li, C.; Uher, C.; Baker Jr, J.R.; Banaszak Holl, M.M.; Orr, B.G. Facile hydrothermal synthesis of iron oxide nanoparticles with tunable magnetic properties. *J. Phys. Chem. C* **2009**, *113*, 13593–13599. [CrossRef]
20. Baimler, I.; Simakin, A.; Uvarov, O.; Volkov, M.Y.; Gudkov, S. Generation of hydroxyl radicals during laser breakdown of aqueous solutions in the presence of Fe and Cu nanoparticles of different sizes. *Phys. Wave Phenom.* **2020**, *28*, 107–110. [CrossRef]
21. Kim, M.; Osone, S.; Kim, T.; Higashi, H.; Seto, T. Synthesis of Nanoparticles by Laser Ablation: A Review. *KONA Powder Part. J.* **2017**, *34*, 80–90. [CrossRef]
22. Ahmadpoor, F.; Masood, A.; Feliu, N.; Parak, W.J.; Shojaosadati, S.A. The Effect of Surface Coating of Iron Oxide Nanoparticles on Magnetic Resonance Imaging Relaxivity. *Front. Nanotechnol.* **2021**, *3*, 644734. [CrossRef]
23. Chausov, D.N.; Smirnova, V.V.; Burmistrov, D.E.; Sarimov, R.M.; Kurilov, A.D.; Astashev, M.E.; Uvarov, O.V.; Dubinin, M.V.; Kozlov, V.A.; Vedunova, M.V. Synthesis of a Novel, Biocompatible and Bacteriostatic Borosiloxane Composition with Silver Oxide Nanoparticles. *Materials* **2022**, *15*, 527. [CrossRef]
24. Ahmad, A.A.; Sarbon, N.M. A comparative study: Physical, mechanical and antibacterial properties of bio-composite gelatin films as influenced by chitosan and zinc oxide nanoparticles incorporation. *Food Biosci.* **2021**, *43*, 101250. [CrossRef]
25. Bharathi, D.; Ranjithkumar, R.; Vasantharaj, S.; Chandarshekar, B.; Bhuvaneshwari, V. Synthesis and characterization of chitosan/iron oxide nanocomposite for biomedical applications. *Int. J. Biol. Macromol.* **2019**, *132*, 880–887. [CrossRef]
26. Dhachanamoorthi, N.; Chandra, L.; Suresh, P.; Perumal, K. Facile preparation and characterization of polyaniline-iron oxide ternary polymer nanocomposites by using "mechanical mixing" approach. *Mech. Mater. Sci. Eng. MMSE J. Open Access* **2017**, *9*, hal-01504671.

27. Das, B.; Chattopadhyay, P.; Upadhyay, A.; Gupta, K.; Mandal, M.; Karak, N. Biophysico-chemical interfacial attributes of Fe$_3$O$_4$ decorated MWCNT nanohybrid/bio-based hyperbranched polyurethane nanocomposite: An antibacterial wound healing material with controlled drug release potential. *New J. Chem.* **2014**, *38*, 4300–4311. [CrossRef]

28. Burmistrov, D.E.; Simakin, A.V.; Smirnova, V.V.; Uvarov, O.V.; Ivashkin, P.I.; Kucherov, R.N.; Ivanov, V.E.; Bruskov, V.I.; Sevostyanov, M.A.; Baikin, A.S. Bacteriostatic and Cytotoxic Properties of Composite Material Based on ZnO Nanoparticles in PLGA Obtained by Low Temperature Method. *Polymers* **2022**, *14*, 49. [CrossRef]

29. Baimler, I.; Simakin, A.; Gudkov, S. Investigation of the laser-induced breakdown plasma, acoustic vibrations and dissociation processes of water molecules caused by laser breakdown of colloidal solutions containing Ni nanoparticles. *Plasma Sources Sci. Technol.* **2021**, *30*, 125015. [CrossRef]

30. Ivanyuk, V.V.; Shkirin, A.V.; Belosludtsev, K.N.; Dubinin, M.V.; Kozlov, V.A.; Bunkin, N.F.; Dorokhov, A.S.; Gudkov, S.V. Influence of Fluoropolymer Film Modified with Nanoscale Photoluminophor on Growth and Development of Plants. *Front. Phys.* **2020**, *8*, 616040. [CrossRef]

31. Kaplan, M.A.; Sergienko, K.V.; Kolmakova, A.A.; Konushkin, S.V.; Baikin, A.S.; Kolmakov, A.G.; Sevostyanov, M.A.; Kulikov, A.V.; Ivanov, V.E.; Belosludtsev, K.N. Development of a biocompatible PLGA polymers capable to release thrombolytic enzyme prourokinase. *J. Biomater. Sci. Polym. Ed.* **2020**, *31*, 1405–1420. [CrossRef]

32. Shtarkman, I.; Gudkov, S.; Chernikov, A.; Bruskov, V. Effect of amino acids on X-ray-induced hydrogen peroxide and hydroxyl radical formation in water and 8-oxoguanine in DNA. *Biochemistry* **2008**, *73*, 470–478. [CrossRef]

33. Gudkov, S.V.; Lyakhov, G.A.; Pustovoy, V.I.; Shcherbakov, I.A. Vibration–Vortex Mechanism of Radical-Reaction Activation in an Aqueous Solution: Physical Analogies. *Phys. Wave Phenom.* **2021**, *29*, 108–113. [CrossRef]

34. Gudkov, S.; Garmash, S.; Shtarkman, I.; Chernikov, A.; Karp, O.; Bruskov, V. Long-lived protein radicals induced by X-ray irradiation are the source of reactive oxygen species in aqueous medium. *Dokl. Biochem. Biophys.* **2010**, *430*, 1. [CrossRef] [PubMed]

35. Sharapov, M.; Novoselov, V.; Penkov, N.; Fesenko, E.; Vedunova, M.; Bruskov, V.; Gudkov, S. Protective and adaptogenic role of peroxiredoxin 2 (Prx2) in neutralization of oxidative stress induced by ionizing radiation. *Free. Radic. Biol. Med.* **2019**, *134*, 76–86. [CrossRef] [PubMed]

36. Gudkov, S.V.; Simakin, A.V.; Sarimov, R.M.; Kurilov, A.D.; Chausov, D.N. Novel Biocompatible with Animal Cells Composite Material Based on Organosilicon Polymers and Fullerenes with Light-Induced Bacteriostatic Properties. *Nanomaterials* **2021**, *11*, 2804. [CrossRef] [PubMed]

37. Gudkov, S.V.; Guryev, E.L.; Gapeyev, A.B.; Sharapov, M.G.; Bunkin, N.F.; Shkirin, A.V.; Zabelina, T.S.; Glinushkin, A.P.; Sevost'yanov, M.A.; Belosludtsev, K.N. Unmodified hydrated C60 fullerene molecules exhibit antioxidant properties, prevent damage to DNA and proteins induced by reactive oxygen species and protect mice against injuries caused by radiation-induced oxidative stress. *Nanomed. Nanotechnol. Biol. Med.* **2019**, *15*, 37–46. [CrossRef]

38. Chausov, D.N.; Burmistrov, D.E.; Kurilov, A.D.; Bunkin, N.F.; Astashev, M.E.; Simakin, A.V.; Vedunova, M.V.; Gudkov, S.V. New Organosilicon Composite Based on Borosiloxane and Zinc Oxide Nanoparticles Inhibits Bacterial Growth, but Does Not Have a Toxic Effect on the Development of Animal Eukaryotic Cells. *Materials* **2021**, *14*, 6281. [CrossRef]

39. Barkhudarov, E. New nanostructured coating of nanosized amorphous carbon inhibits bacterial growth, but does not have a toxic effect on the development of animal eukaryotic cells. *Nanomaterials* **2020**, *10*, 2130. [CrossRef]

40. Gudkov, S.V.; Simakin, A.V.; Bunkin, N.F.; Shafeev, G.A.; Astashev, M.E.; Glinushkin, A.P.; Grinberg, M.A.; Vodeneev, V.A. Development and application of photoconversion fluoropolymer films for greenhouses located at high or polar latitudes. *J. Photochem. Photobiol. B Biol.* **2020**, *213*, 112056. [CrossRef]

41. Burmistrov, D.E.; Yanykin, D.V.; Simakin, A.V.; Paskhin, M.O.; Ivanyuk, V.V.; Kuznetsov, S.V.; Ermakova, J.A.; Alexandrov, A.A.; Gudkov, S.V. Cultivation of Solanum lycopersicum under Glass Coated with Nanosized Upconversion Luminophore. *Appl. Sci.* **2021**, *11*, 10726. [CrossRef]

42. Gudkov, S.V.; Simakin, A.V.; Konushkin, S.V.; Ivannikov, A.Y.; Nasakina, E.O.; Shatova, L.A.; Kolmakov, A.G.; Sevostyanov, M.A. Preparation, structural and microstructural characterization of Ti–30Nb–10Ta–5Zr alloy for biomedical applications. *J. Mater. Res. Technol.* **2020**, *9*, 16018–16028. [CrossRef]

43. Sevostyanov, M.A.; Kolmakov, A.G.; Sergiyenko, K.V.; Kaplan, M.A.; Baikin, A.S.; Gudkov, S.V. Mechanical, physical–chemical and biological properties of the new Ti–30Nb–13Ta–5Zr alloy. *J. Mater. Sci.* **2020**, *55*, 14516–14529. [CrossRef]

44. Konushkin, S.V.; Sergiyenko, K.V.; Nasakina, E.O.; Leontyev, V.G.; Kuznetsova, O.G.; Titov, D.D.; Tsareva, A.M.; Dormidontov, N.A.; Kirsankin, A.A.; Kannykin, S.V. Study of the physicochemical and biological properties of the new promising Ti–20Nb–13Ta–5Zr alloy for biomedical applications. *Mater. Chem. Phys.* **2020**, *255*, 123557. [CrossRef]

45. Ezealigo, U.S.; Ezealigo, B.N.; Aisida, S.O.; Ezema, F.I. Iron oxide nanoparticles in biological systems: Antibacterial and toxicology perspective. *JCIS Open* **2021**, *4*, 100027. [CrossRef]

46. Cotin, G.; Kiefer, C.; Perton, F.; Ihiawakrim, D.; Blanco-Andujar, C.; Moldovan, S.; Lefevre, C.; Ersen, O.; Pichon, B.; Mertz, D.; et al. Unravelling the Thermal Decomposition Parameters for The Synthesis of Anisotropic Iron Oxide Nanoparticles. *Nanomaterials* **2018**, *8*, 881. [CrossRef]

47. Hufschmid, R.; Arami, H.; Ferguson, R.M.; Gonzales, M.; Teeman, E.; Brush, L.N.; Browning, N.D.; Krishnan, K.M. Synthesis of phase-pure and monodisperse iron oxide nanoparticles by thermal decomposition. *Nanoscale* **2015**, *7*, 11142–11154. [CrossRef]

48. Belaïd, S.; Laurent, S.; Vermeersch, M.; Vander Elst, L.; Perez-Morga, D.; Muller, R.N. A new approach to follow the formation of iron oxide nanoparticles synthesized by thermal decomposition. *Nanotechnology* **2013**, *24*, 055705. [CrossRef]

49. Arakha, M.; Pal, S.; Samantarrai, D.; Panigrahi, T.K.; Mallick, B.C.; Pramanik, K.; Mallick, B.; Jha, S. Antimicrobial activity of iron oxide nanoparticle upon modulation of nanoparticle-bacteria interface. *Sci. Rep.* **2015**, *5*, 14813. [CrossRef]

50. Sevcu, A.; Cernik, M. Oxidative stress in microorganisms exposed to iron nanoparticles. *WIT Trans. Ecol. Environ.* **2010**, *141*, 97–107.

51. Touati, D. Iron and oxidative stress in bacteria. *Arch. Biochem. Biophys.* **2000**, *373*, 1518. [CrossRef]

52. Collins, A. Comparison of different methods of measuring 8-oxoguanine as a marker of oxidative DNA damage. *Free. Radic. Res.* **2000**, *32*, 333–341. [CrossRef]

53. Nehra, P.; Chauhan, R.; Garg, N.; Verma, K. Antibacterial and antifungal activity of chitosan coated iron oxide nanoparticles. *Br. J. Biomed. Sci.* **2018**, *75*, 13–18. [CrossRef]

54. Nguyen, D.T.; Pham, L.T.; Le, H.T.; Vu, M.X.; Le, H.T.; Le, H.T.; Pham, N.H.; Lu, L.T. Synthesis and antibacterial properties of a novel magnetic nanocomposite prepared from spent pickling liquors and polyguanidine. *RSC Adv.* **2018**, *8*, 19707–19712. [CrossRef]

55. Kavitha, A.; Prabu, H.G.; Babu, S.A. Synthesis of low-cost iron oxide: Chitosan nanocomposite for antibacterial activity. *Int. J. Polym. Mater.* **2013**, *62*, 45–49. [CrossRef]

56. Dhivya, S.M.; Sathiya, S.; Manivannan, G.; Rajan, M.J. A comparative study on the biopolymer functionalized iron oxide nanocomposite for antimicrobial activity. *Mater. Today Proc.* **2016**, *3*, 3866–3871. [CrossRef]

57. Diez-Pascual, A.M. Antibacterial Nanocomposites Based on Thermosetting Polymers Derived from Vegetable Oils and Metal Oxide Nanoparticles. *Polymers* **2019**, *11*, 1790. [CrossRef]

58. Jeong, C.J.; Sharker, S.M.; In, I.; Park, S.Y. Iron oxide@ PEDOT-based recyclable photothermal nanoparticles with poly (vinylpyrrolidone) sulfobetaines for rapid and effective antibacterial activity. *ACS Appl. Mater. Interfaces* **2015**, *7*, 9469–9478. [CrossRef]

59. Chen, X.; Hu, B.; Xiang, Q.; Yong, C.; Liu, Z.; Xing, X. Magnetic nanoparticles modified with quaternarized N-halamine based polymer and their antibacterial properties. *J. Biomater. Sci. Polym. Ed.* **2016**, *27*, 1187–1199. [CrossRef]